Nanoscale

Accepted Manuscript

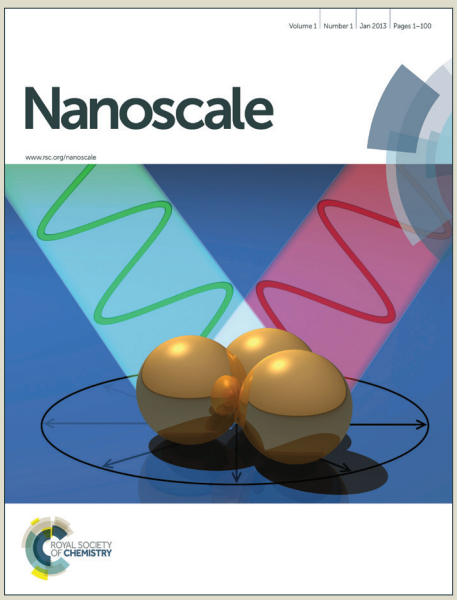

ROYAL SOCIETY OF CHEMISTRY

www.rsc.org/nanoscale

Journal Name

RSCPublishing

ARTICLE

Where is the required lattice match in horizontal growth of nanowires?

Cite this: DOI: 10.1039/x0xx00000x

Babak Nikoobakht,*[a] Andrew Herzing [a]

Received ooth January 2012,
Accepted ooth January 2012

DOI: 10.1039/x0xx00000x

www.rsc.org/

The horizontal growth of nanowires (NWs) using the surface-directed vapor-liquid-solid (SVLS) process has been demonstrated for a number of semiconductors and shows the unique ability of eliminating post-growth alignment steps. However, the epitaxial relationship between horizontal NWs and their underlying surface has not been well understood, as it becomes more convoluted in systems with closely matched lattice and crystal symmetry. We have unraveled one of the main mechanisms driving the lateral growth by investigating a highly-mismatched system comprising TiO_2 anatase, a 4-fold symmetry crystal, grown on substrates with lower and higher symmetries including sapphire and GaN. Counter-intuitively, our results reveal that the lattice match with substrate exists along the width of the NWs. We demonstrate the first set of examples that rule out the requirement for having a lattice match along the NW growth axis, which is observed in the non-VLS growth of epitaxial quantum wires. Unlike wurtzite or zinc-blende crystals that have a preferred lattice orientation regardless of the substrate crystal structure, we observe new evidence on strict control of the substrate on shape, faceting and orientation of nanocrystals that could offer a selective route for tailoring TiO_2 NW properties and functions at the ensemble level.

Introduction

Controlled, horizontal growth of NWs is of interest because it can eliminate the need for post-growth assembly and offers a direct route for integration with planar device designs. Metal-catalyzed horizontal growth using the SVLS mechanism is an epitaxial process in which one-dimensional (1D) nanocrystals grow on a single crystal surface forming in-situ assemblies[1-3] with predictable hierarchies and NW registries.[4-6] Full utilization of this growth process requires understanding the mechanisms and forces that guide the growth, which is considered a key technological step impacting the future of nanointegration in advanced materials and devices.

Intrinsic information on a single crystal surface has been used by crystal growers for decades to form epitaxial layers. This type of growth has been used in its super-confined form in the VLS growth process where a metal catalyst acts as a material concentrator resulting in rapid and localized growth of free-standing NWs at specific sites.[7-10] Previously, we extended this concept to the lateral growth of semiconductor NWs on single crystal substrates using the SVLS process.[1] Results and proposed models suggest that the initial crystal seed is formed at the vapor-liquid-solid interface, however, it does not spread over the whole liquid-solid (metal/substrate) interface (Figure 1) despite what occurs in the free-standing VLS growth.[11, 12] As a result during the growth, the metal droplet maintains its interface with the substrate while undergoing cycles of supersaturation and depletion due to nanocrystal precipitation. The nanocrystal precipitates at one side of the metal droplet and advances the metal droplet forward where a new nanocrystal forms. Repetition of this sequential island growth results in the formation of horizontal NWs. The key distinction in the SVLS process is that it is simultaneously influenced by two growth fronts involving the semiconductor/metal and semiconductor/substrate interfaces, which are not co-planar as schematically shown in Figure 1 (highlighted in blue and green colours). This compound interface could enable interesting crystal growth phenomena that otherwise cannot be observed in conventional crystal growth settings.

In this report, we have investigated the heteroepitaxy of NWs in systems where both lattice symmetry and lattice match are intentionally selected to be low in order to reveal any relationships that have remained obscure in the lattice matched systems. The present report demonstrates evidence that discounts the need for lattice match along the growth axis of laterally grown NWs. We also show examples in which a change in substrate symmetry forces the growth axis symmetry of the nanocrystal lattice to change in compliance with the underlying surface.

In planar growth of quantum wires or quasi-one-dimensional islands using the vapor-solid (VS) growth processes, it is shown that an island elongates in the direction

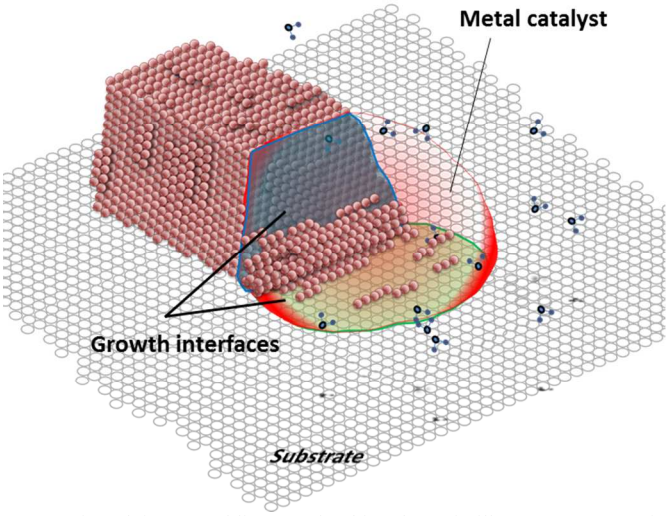

Fig. 1 Viewed from an oblique angle, this schematic illustrates a NW at its early stage of growth via the SVLS process. The resulting nanocrystal does not spread across the gold-substrate interface and its packing is defined by both the gold/semiconductor (blue face) and gold/substrate interfaces (green face).

that is closely lattice matched to the substrate and has a limited growth along the perpendicular axis where it has a significant mismatch.[3, 13] Film stress[14] and surface stress[15] have been used to explain the observed anisotropy in the growth and have been exploited to grow NWs in plane of the substrate.[16] In thin film growth, island formation has been described as a mechanism for strain relaxation without dislocation formation.[17, 18] In islands where strain is not isotropic, it is shown that the elongation occurs along the direction that has a lower strain.[14] For instance, in lateral growth of CaF_2 on Si (001) 2 % and 45 % lattice mismatches exist along the island length and width, respectively.[3] The drawback of this approach is that it can only be applied to a limited number of material combinations, as well as the lack of predictability of the NW growth sites.[15]

Similarly, in the SVLS growth of NWs, the same understanding has been applied to account for the anisotropic island growth. Thus far, horizontal growth has been shown for some of the II-VI, III-V and IV semiconductor NWs, including ZnO on *a*-sapphire,[1] GaAs on GaAs,[2] ZnO on GaN, [5] Mg_2SiO_4 on Si,[19] GaN on sapphire,[20, 21] and Ge on Ge. [22] The common characteristic in all of these systems is that both nanocrystal and substrate belong to the same crystal family with a lattice mismatch of less than 3 %. The resulting NWs are highly-lattice matched with the substrate along both their length and width, which makes it difficult to determine the direction in which lattice match is more essential in driving the planar epitaxial growth.

In this report, we investigate the lateral growth of oxide semiconductor NWs where the lattice constants and crystal symmetries are mismatched. The semiconductor of choice, TiO_2, is a tetragonal crystal (4-fold symmetry) that is horizontally grown on GaN and *a*-plane sapphire substrates which exhibit higher and lower crystal symmetries of 6- and 2-fold, respectively.

TiO_2 has been widely used and investigated in a multitude of applications including photocatalysis, gas sensing, detoxification, solar cells, and transparent conductive electrodes.[23-25] TiO_2 is typically crystalized in three different polymorphs: anatase, brookite, and rutile. High quality rutile has been more readily available than anatase, although the latter has been shown to be more important for several reactions including the photocatalytic formation of H_2 and O_2 from water.[26] Single crystalline TiO_2 is also considered superior to polycrystalline materials in applications where charge transport is necessary since grain boundaries and defects can cause scattering or degradation of the mobility of charge carriers.[25] Therefore, for technological applications it is very important to develop methods for controlled formation of TiO_2 crystal phases and single crystalline structures that have well-defined crystal facets.

Previous work on thin film growth of TiO_2 shows that high temperature growth ranging from 400 °C to 1200 °C promotes the anatase-to-rutile transformation, primarily due to the increase in the crystal grain size.[27] In addition, the rutile formation seems to be independent of the substrate as it has been observed on a variety of surfaces including the $(1\bar{1}02)$ and (0001) sapphire,[28, 29] quartz,[30] glass[31] and silicon[25]. In the case of TiO_2 nanostructures, this effect has also resulted in a mixed population containing both anatase and rutile phases.[32] However, for arrays of TiO_2 nanodots less than 60 nm in diameter, it is shown that anatase is the dominant phase since the nanocrystal size is smaller than the grain size required for rutile formation.[33-35] In this report, while investigating the in-plane epitaxial growth of 1D TiO_2 nanocrystals, we also observe that the nanocrystal lattice symmetry of NWs and thus their out-of-plane growth direction is directly controlled by the lattice symmetry of the underlying substrates.

Results and discussion

The SVLS growth of NWs is carried out in a horizontal tube furnace with 800 mm length and 49 mm inner diameter. A titanium oxide/graphite mixture (0.15 g, 1:1 mass ratio) is positioned inside and at the center of a small quartz tube that has 130 mm length and 19 mm inner diameter. 10 nm to 20 nm thick thermally evaporated gold patterns on *a*-sapphire or GaN are placed at the end of the small tube downstream of the carrier gas. The tube furnace temperature is set at 900 ºC (with a ramp rate of 110 ºC/min.) for dwell times ranging from 10 minutes to 35 minutes. The actual tube temperature at its growth zone could briefly reach to 1000 ºC due to overheating. During the growth, the tube remains under 0.59 standard liters per minute (SLPM) flow of ultra-dry N_2 gas (99.99%). We use two different starting materials of titanium oxide (Ti_2O_3) and titanium dioxide (TiO_2) for growth of NWs. The NW cross-sections were made and polished using a focused ion beam (FIB) instrument.[36] Bulk crystal lattice indexing and diffraction pattern simulations were performed using Crystal Maker.*

During the growth process, as the temperature reaches 600 °C to 700 °C the gold film pattern transforms to nanodroplets. Therefore, once at the growth temperature of 900 ºC, it is reasonable to consider a VLS-based growth mechanism for crystallization of TiO_2 NWs. It is important to note that the formed gold droplets within the pattern interior result in standing NWs and those at the periphery of the pattern result in horizontal NWs.[5] Top and side views of such assemblies are shown in Figures 2 (a-b). Horizontal NWs show thicknesses ranging from 10 nm to 20 nm, while the free standing ones are 35 nm or thicker.

* Certain commercial equipment, instruments, or materials are identified in this paper to adequately specify the experimental procedure. In no case does such identification imply recommendation or endorsement by the National Institute of Standards and Technology, nor does it imply that the materials or equipment identified are necessarily the best available for the purpose.

Similar to very thin epilayers, in-plane structural characterization of horizontal TiO_2 NWs is challenging since their lattice constant typically complies with the underlying substrate. In this regard, we examined NW cross-sections from different perspectives, i.e., in substrate plane as well as along their width and growth axes.

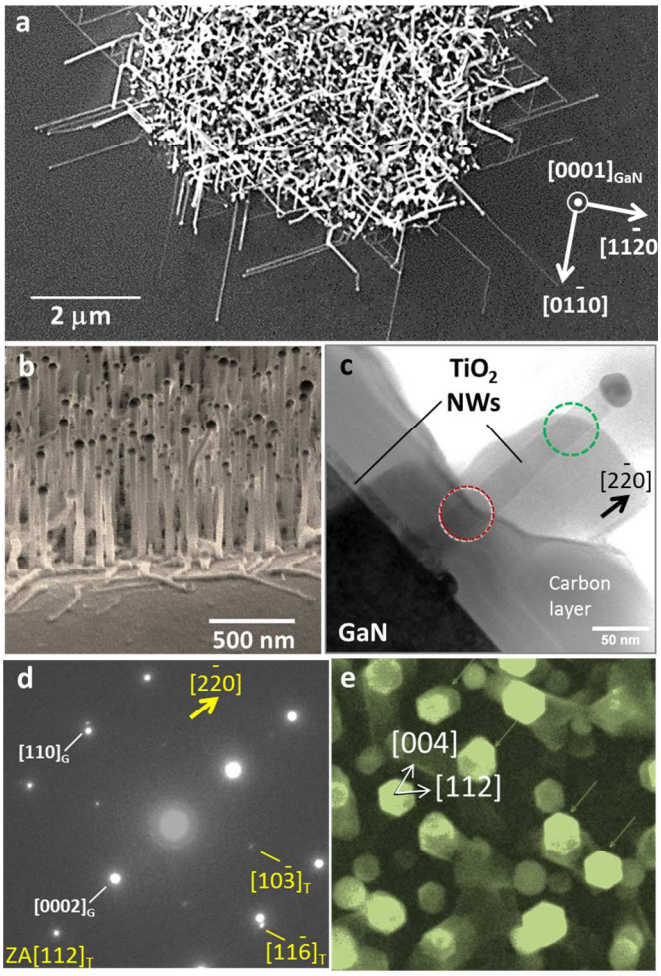

Fig. 2 Top (a) and side (b) view micrographs of upright TiO_2 NWs grown on (0001) GaN. The top view shows the directed growth of horizontally grown TiO_2 NWs at the periphery of a gold pattern. Cross-section of part of this area is shown in HR-TEM image of (c), which includes an upright and horizontal NW attached to the GaN surface. d) SAED pattern collected from the interface of NWs/GaN shows diffraction spots of TiO_2 (denoted as T) and GaN (denoted as G). Note that in the anatase structure, the unit cell in the c direction is elongated such that it makes the [112] and $[\bar{1}16]$ orthogonal (supporting information). e) Top view micrograph of the upright NWs shows six sides with facet angles of about 60°.

Figure 2c shows a cross-sectional high resolution transmission electron microscope (HR-TEM) image of representative NWs selected from the region shown in Figure 2a that includes two upright and horizontal NWs. To better reveal any strain patterns in the NWs, crystal lattice of the upright one was examined using HR-TEM. Starting from top at the vicinity of the metal catalyst (green circle) to about 50 nm above the interface (red circle), the NW lattice maintains its bulk lattice dimensions with a plane spacing of 0.13 nm along the growth axis indicating a strain-free structure with a growth direction of $[2\bar{2}0]$ which agrees well with the simulated bulk TiO_2 anatase structure (Fig.S1). However, selected area electron diffraction (SAED) pattern of the interface presented in Figure 2d containing part of the horizontal NW and base of the upright NW shows a plane spacing of 0.11 nm signifying a TiO_2 lattice compression along the out-of-plane growth axis (Fig.S1). The upright NWs viewed from top in Figure 2e show a 6-sided cross-section which agrees with its $[2\bar{2}0]$ growth axis deduced from HR-TEM. To further confirm the lattice orientation of the horizontal TiO_2 NWs, its cross-section along the NW width was examined using HR-TEM as shown in Figure 3. Examination of the TiO_2 lattice spacing along the surface normal shows a spacing of 0.11 nm indicating a slight lattice compression relative to the bulk value, which is in agreement with the lattice compression observed in the SAED data of Figure 2d. Previously, in the case of horizontal ZnO NWs on *a*-sapphire a similar strain pattern was observed as well.[36] Figure 3 and inset also reveal the NW side facets, namely, $(3\bar{1}2)$ and (112) relative to the NW growth axis and further supports the anatase structure.

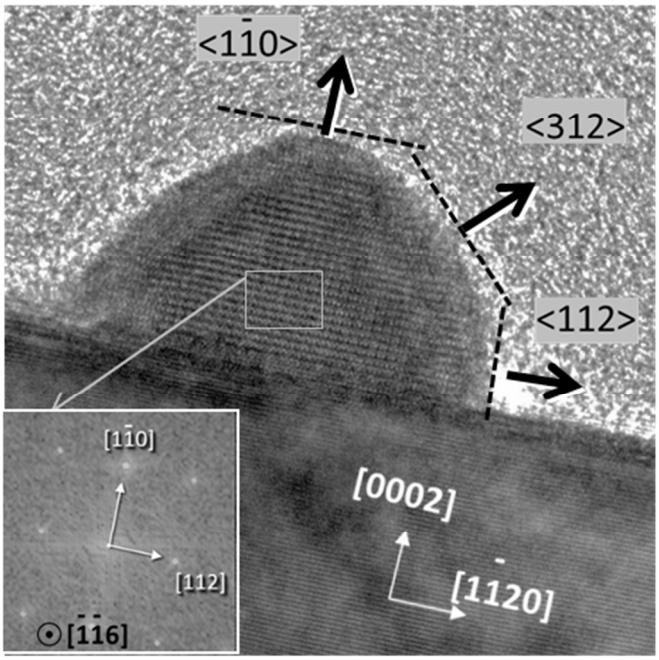

Fig. 3 a) Cross-sectional HR-TEM image of a horizontal TiO_2 NW on GaN. The inset FFT pattern highlights the NW side facets and its ZA of $[\bar{1}16]$. The crystallographic orientation of TiO_2 NW relative to the GaN substrate is also illustrated.

Horizontal NWs were also examined from top view using HR-TEM to determine their in-plane lattice orientation relative to the GaN substrate. Figure 4a shows a specimen prepared for HR-TEM imaging that contains two NWs grown on the basal plane of GaN and Figure 4b illustrates its SAED pattern. The strong diffraction spots with 6-fold symmetry correspond to the GaN *m*- and *a*-planes, indexed as $[0\bar{1}10]$ and $[\bar{2}110]$, respectively. The weaker spots with a similar symmetry correspond to the reflections of TiO_2 NWs suggesting the out-of-plane $[2\bar{2}0]$ growth axis of horizontal NWs. Comparing the SAED data with the bulk values shows that the $(\bar{2}\bar{2}4)$ and $(00\bar{8})$ TiO_2 planes expand in the GaN basal plane. As a result, the lattice spacing along the width of the NW expands from 0.23 nm to 0.28 nm. This observation also agrees with the NW lattice compression in its $[1\bar{1}0]$, out-of-plane, growth direction.

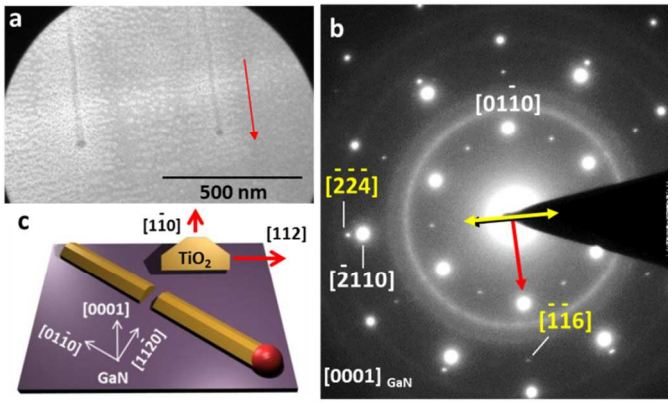

Fig. 4 a) HR-TEM image of an in-plane section of laterally grown TiO_2 NWs on (0001) GaN and (b) its corresponding SAED pattern. Along the width of the NW (yellow arrow), diffraction spots of $(\overline{224})$ and $(\bar{2}110)$ show a closer agreement than what is seen along the growth direction of the NW (red arrow). The diffraction rings are due to the deposited Pt on the specimen. c) Schematic of NWs side facets and its orientation relative to the substrate crystallographic directions.

The proximity of the $(\overline{224})$ and $(\bar{2}110)$ diffraction spots along the NW width highlights formation of a pseudo-lattice match in the GaN *a*-direction. The 6-fold symmetry of $[\bar{2}110]$ direction results in the 6-fold rotational symmetry of the NW growth directions as is shown experimentally in Figure 2a. This observation demonstrates that it is the symmetry of a specific crystallographic direction of the substrate that defines the growth symmetry of NWs and not the crystal symmetry of the NWs themselves. The position of the extracted NW specimen is schematically shown in Figure 4c in which the overall NW lattice orientation relative to the GaN crystallographic axes is $[112]\ TiO_2 \parallel [1\bar{1}20]_{GaN}$.

The pseudo-lattice matched direction along the NW width shown with yellow arrow in Figure 4b is remarkable as it also shows no lattice match exists along the NW growth axis (same figure, red arrow). This observation conflicts with the current understanding of anisotropic island growth in the non-VLS growth processes. In the non-VLS lateral growth of NWs, it is experimentally and theoretically established that the lattice match occurs along the length of the NWs. This growth mechanism has been implicitly extended to the VLS-based growth of horizontal NWs as well. The SAED pattern of Figure 4b is a clear example of the absence of any lattice match along the $[\bar{1}16]$ growth axis of the NW.

To further confirm these observations, the lateral growth of TiO_2 was also investigated on *a*-sapphire, which exhibits a lower symmetry (2-fold) than *c*-GaN. In this case, the substrate guides the NW growth in directions with a 2-fold rotational symmetry as shown in Figure 5a (Figure S2). Representative 2θ XRD pattern of the horizontal NWs in Figure 5b was collected using a Bruker D8 equipped with a Vantec2000 2D detector. The 2D diffraction frames were collected at a theta-theta arrangement. The XRD scans show reflections at 37.8° and 38.2° which are assigned to $(11\bar{2}0)$ and (112) reflections of *a*-sapphire and anatase TiO_2, respectively. This shows that the dominant out-of-plane growth direction in the laterally grown NWs on *a*-sapphire is [112], while it was $[2\bar{2}0]$ in the case of GaN substrate. To further understand the relationship and orientation order between the two crystals, in-plane sections of a group of laterally grown NWs on *a*-sapphire were prepared using FIB (Figure S2c).

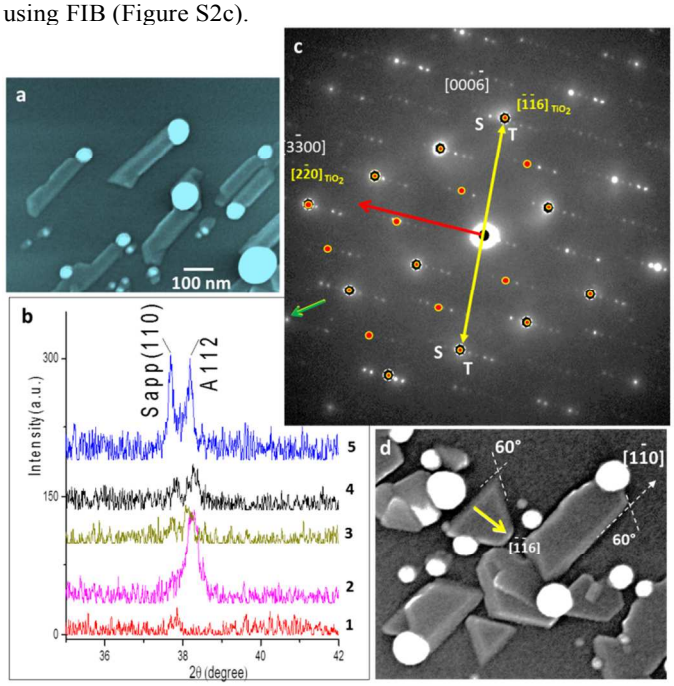

Fig. 5 a) Top view micrograph of laterally grown TiO_2 NWs on *a*-plane sapphire. NWs are about 40 nm wide and 25 nm thick. b) Signature 2θ-XRD shows reflections of (112) plane of TiO_2 NWs and (110) sapphire plane. Spectrum 1 belongs to only *a*-sapphire; spectra 2-5 are collected in multiple runs from horizontal NWs grown on *a*-sapphire. c) SAED pattern of the in-plane section of TiO_2 NWs on *a*-plane sapphire (image shown in Fig.S2c). Dark and red circles correspond to sapphire and TiO_2 reflections, respectively. Only along yellow arrow direction, the ED spots of the two crystals overlap indicating lattice match in this direction. This is shown at ED spots labelled with "S" and "T", which denote sapphire and TiO_2, respectively. d) NWs can also grow along their width via a non-VLS process to form 2D nanocrystals. This growth is only observed at side facets and orthogonal to the NW growth direction.

The SAED pattern of this collection in Figure 5c shows the more pronounced *a*-sapphire reflections corresponding to the $[1\bar{1}20]$ zone axis (represented by dark circles). The weaker SAED reflections correspond to the TiO_2 NWs that are also accompanied by adjacent 'satellite' spots along the growth axis of the NWs (red arrow). More on these 'satellite' patterns will be discussed later.

For clarity the diffraction spots of TiO_2 unit cell are highlighted with red circles to show the orientation of TiO_2 unit cell in the *a*-plane of sapphire. Because of the small NW thickness of less than 25 nm, TiO_2 essentially takes the lattice constant of the sapphire, which makes the SAED pattern indexing more difficult. Due to its lattice expansion, TiO_2 ED spots (labeled as "T") overlap with those of sapphire (marked as "S") along the <0006> of sapphire, which precisely coincides with the transverse direction of the NW (yellow arrow). The $<0006>_{Sap}$ direction has a 2-fold symmetry, which explains why a 2-fold symmetry is observed for growth directions of NWs. It is noteworthy to point out that the ZnO NWs grow in the same crystallographic direction of sapphire.[1]

In addition to crystal diffraction analysis, we use morphology analysis of the nanocrystals to further understand their crystal structure and variation relative to its bulk. Figure 5d shows that TiO_2 NWs undergo a side growth via a non-VLS process resulting in planar nanostructures (Fig. S3). This morphology illustrates a

secondary nanocrystal growth direction orthogonal to the NW growth axis, which is shown with yellow arrow. Small clusters of Au or Au-O as impurities along with non-stoichiometric ratios of Ti and O are likely candidates in promoting the observed side growth.[37] The side growth results in dominantly 4-sided nanocrystals with trapezoid shape that can also grow to truncated triangles. It is noted that the surface area of the surrounding facets change but their angles are preserved. From top view, facet angle measurements in the plane of substrate show 60° and 120° for acute and obtuse angles, respectively, which are in close agreement with those of the TiO_2 bulk at a similar orientation. Examining the nanocrystals along their length using cross-sectional HR-TEM as depicted in Figures 6a-b shows the $(\bar{1}32)$ plane with an angle of 60° relative to the (112) plane (which is parallel to the surface).

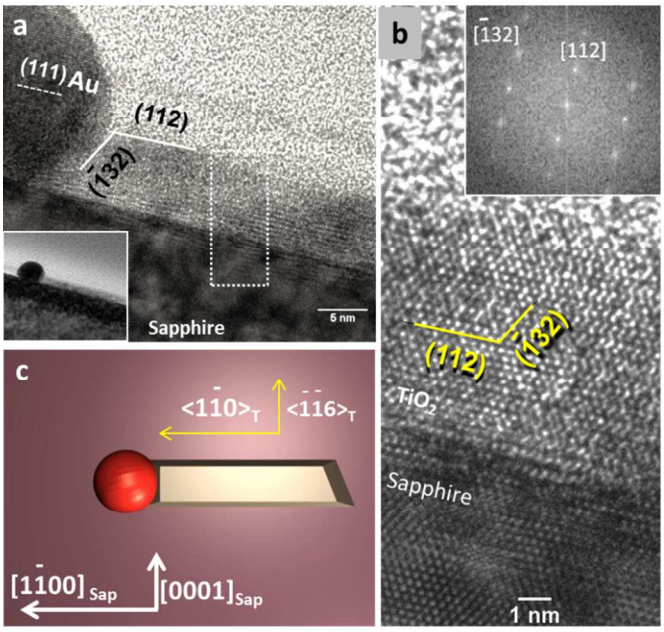

Fig. 6 a) Cross-sectional HR-TEM image along TiO_2 NW length where it interfaces with the gold catalyst. Inset shows a lower magnification of this cross-section and (b) shows the lattice resolved TEM image of the marked box in part (a). The inset FFT pattern shows that the (112) and $(\bar{1}32)$ planes are, respectively, parallel and 60° tilted relative to the substrate. These planes are also shown in part (a) with respect to the gold catalyst. c) Orientation of a TiO_2 NW relative to the *a*-sapphire crystallographic directions.

The $\{\bar{1}32\}$ family of planes, as shown in Figure 6b, is likely to possess an interface with the gold melt and therefore be the growth front of the NW in $<1\bar{1}0>$. Based on this model, as illustrated in Figure 6c, the two NW side facets are (220) and (116) planes and the in-plane orientation order of TiO_2 on *a*-sapphire is likely to be $<\bar{1}\bar{1}6>_{TiO2} \parallel <0001>_{Sapp}$. Figure 6a also shows that the gold melt at the leading end of the NW crystalizes in a *fcc* structure with the typical out-of-plane growth direction of [111]. However, in the case of gold catalyst on upright TiO_2 NWs, this direction is found to be [001] (Fig.S4).

Similar to the observations for horizontal TiO_2 NWs on GaN, no lattice commensuration was detected between TiO_2 and sapphire along the growth direction of the NWs, i.e., $[2\bar{2}0]$. Nonetheless, as seen in Figure 7a, a highly periodic structure is observed along the growth axis of the NWs grown on *a*-sapphire, which is absent in the case of TiO_2 NWs on GaN. HR-TEM cross-sectional analysis of these NWs shows a relaxed lattice in the out-of-plane [112] direction of NWs as its 0.23 nm (±0.1 nm) spacing remains fairly close to the bulk value of 0.23 nm. On the other hand, based on the SAED pattern of Figure 5c, the TiO_2 unit cell expands in the substrate plane to reduce its mismatch. However, examining the SAED pattern along the NW growth axis (red arrow) shows that the in-plane lattice stretch is localized and only alternative atomic planes of TiO_2 overlap with the sapphire planes.

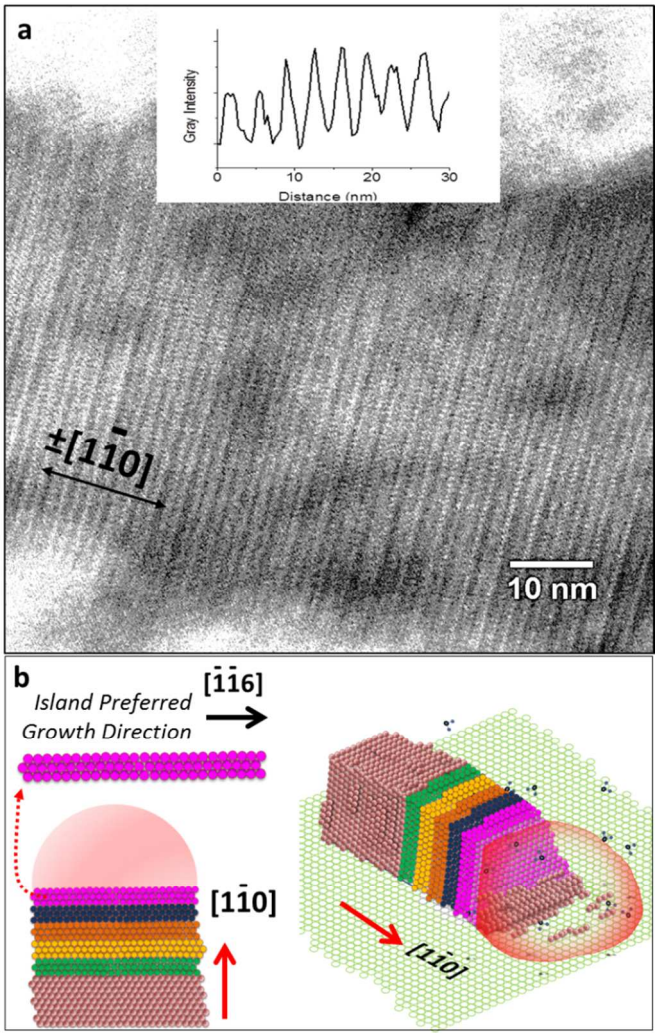

Fig. 7 a) HR-TEM image of an in-plane section of a laterally grown TiO_2 NW on *a*-plane sapphire, where a super cell is formed along the growth direction. Inset shows a line profile along the growth direction highlighting a periodicity of 5 to 7 nm. b) Left schematic depicts thin NW segments (coloured) that grow along the preferred growth direction of the nanocrystal. These segments are formed orthogonal to the NW growth axis. Different colours are used to schematically show the sequential island growth. Right schematic illustrates the NW from an oblique view.

Therefore, the observed superlattice could be due to the formation of an ordered array of misfit dislocations for releasing the lattice strain along the NW growth axis.[38] The periodic structure could also be a translational Moirė pattern, which could accompany the misfit dislocations. This effect can be shaped due to interference of two overlaid patterns that have common periodicities. This process is an example of double diffraction, in which a diffracted electron from the top crystal acts as an incident beam for a second

diffraction in the underlying layer.[39] The spacing among 'satellite' diffraction patterns shows a lattice constant that uniformly alternates between 5.7 nm and 7.1 nm along the NW growth axis that also agrees with the measured spacing shown in the inset of Figure 7a. Alternatively, the observed interference pattern could be just a double diffraction effect in the absence of any misfit dislocations. The lack of any periodic structure in the HRTEM cross-section of NWs along their length (Fig. 6b) is supportive of the latter explanation; however, more detailed structural analysis is underway to understand this effect.

As stated earlier, in the lateral growth of NWs using the non-VLS processes, the long axis of the nanocrystal is the direction that has a better lattice match with underlying substrate. In contrast, our results show a far better lattice match along the NW width. This contradiction can be explained as follows: during the SVLS growth process, each super saturation and crystallization results in a thin island, schematically, highlighted in Figure 7b. The island grows along a preferred growth direction, where the two crystals show a pseudo-lattice match (in the TiO_2 case this is $[\bar{1}16]$). Energetically, the gold melt favors forming an interface with the long side of the island, which could contain facets such as $(\bar{1}32)$. Therefore, the long side of the island is in contact with the gold droplet and always remains larger than its thickness. As a result of this configuration, the gold melt is forced to move orthogonally to the preferred direction of the TiO_2 island, i.e., $<\bar{1}16>$. The observed side growth of NWs shown in Figure 5d further supports the lattice match along this direction.

In better matched systems such as ZnO on GaN (1.9 % mismatch) the sequential island growth shows islands about 12 nm to 20 nm in length that assemble continuously and form single crystal NWs with low defect densities.[40] In the case of TiO_2 on *a*-sapphire, because of the observed mismatch, a smaller island thickness and junction coherency length are expected. Therefore, it is plausible to assume that the thickness of the island is in the order of periodicity of the observed superlattice (5-7 nm).

One important question raised by these findings is whether it is possible to theoretically predict the occurrence of lateral growth in other semiconductors in combination with the appropriate substrates. At this point, experimental observation remains the best approach for identifying lateral growth in other material combinations. This is because comparison of bulk lattice parameters of TiO_2 on both *a*-sapphire and GaN along the experimentally observed growth direction does not show any proportionality in their lattice planes.

The substrate impact is less obvious in the case of the growth of wurtzite crystals such as ZnO NWs on both aforementioned substrates, where only [0001] out-of-plane growth direction is observed.[40, 41] In other semiconductors including InP grown on Si (111) or InAs on GaAs, the dominant growth direction also remains unique, i.e., [111], independent of the substrate crystal symmetry.[8, 42] There are reports of a change in NW growth direction in such systems, however, this has been proposed as a mechanism to reduce the residual compressive strain at the base of the NWs and not a direct substrate influence.[43, 44] In the case of TiO_2 NWs, the substrate impacts the orientation of the TiO_2 unit cell resulting in growth of single crystal TiO_2 anatase phase with controlled crystal facets. On GaN, the out-of-plane growth direction is found to be $[2\bar{2}0]$ and on *a*-sapphire is [112]. Interestingly, in the former case, the TiO_2 nanocrystal nearly has a 6-fold lattice symmetry and in the latter a 2-fold symmetry. These symmetries are identical to those of their underlying surfaces showing the substrate influence on packing order of the overgrown nanostructures.

Conclusions

In this report, it was shown that the symmetry of a specific crystallographic direction of substrate at which the two lattices match defines the growth symmetry of NWs. This relationship was found to exist along the width of a NW and is proposed to be the minimum requirement for observing the SVLS growth. This epitaxial relationship is believed to drive the lateral growth of NWs, although remains obscure in systems such as ZnO on GaN, where good lattice matches exist along multiple crystallographic directions. Results show anatase TiO_2 nanocrystals maintain their tetragonal crystal structure on both substrates, but they expand in-plane of the substrate. By changing the substrate from GaN to *a*-sapphire, the out-of-plane growth direction of the nanocrystal changes from $[2\bar{2}0]$ to [112] resulting in a reduction in the number of facets surrounding the nanocrystal from six to four. These results offer a potential route for producing tailored NW surfaces and crystal facets for catalytic applications. The sequential island growth is also expected to offer novel capabilities in growth of highly-mismatched semiconductors that are unlikely to materialize in conventional crystal growth processes. In this regard, exploiting surface information of crystals such as differences in lattice match and symmetry to control structure and direction of 1D- nanocrystals offers an advantageous toolset for structural alteration and parallel integration of nanodevices on a large scale.

Acknowledgements

A portion of the nanofabrication in this study was performed at the NIST Center for Nanoscale Science and Technology.

Notes and references

[a] Material Measurement Science Division, National Institute of Standards and Technology, Mailstop 8372, Gaithersburg, 20899, MD, USA..

* E-mail: babak.nikoobakht@nist.gov (Author to whom correspondence should be addressed.)

Electronic Supplementary Information (ESI) available: [details of any supplementary information available should be included here]. See DOI: 10.1039/b000000x/

1. B. Nikoobakht, C. A. Michaels, S. J. Stranick and M. D. Vaudin, *Applied Physics Letters*, 2004, **85**, 3244-3246.
2. S. A. Fortuna, J. Wen, I. S. Chun and X. Li, *Nano Letters*, 2008, **8**, 4421-4427.
3. D. Loretto, F. M. Ross and C. A. Lucas, *Applied Physics Letters*, 1996, **68**, 2363-2365.
4. B. Nikoobakht, *Chemistry of Materials*, 2007, **19**, 5279-5284.
5. B. Nikoobakht and A. Herzing, *ACS Nano*, 2010, **4**, 5877-5886.
6. M. Schvartzman, D. Tsivion, D. Mahalu, O. Raslin and E. Joselevich, *Proceedings of the National Academy of Sciences*, 2013.
7. P. L. Edwards and R. J. Happel, *Journal of Applied Physics*, 1962, **33**, 943-948.
8. R. S. Wagner and W. C. Ellis, *Appl. Phys. Lett.*, 1964, **4**, 89-90.
9. Y. Miyamoto and M. Hirata, *Japanese Journal of Applied Physics*, 1975, **14**, 1419-1420.

10. E. I. Givargizov, *Highly Anisotropic Crystals*, Kluwer Academic Publishers, 1987.
11. I. P. Soshnikov, G. E. Cirlin, A. A. Tonkikh, Y. B. Samsonenko, V. G. Dubovskii, V. M. Ustinov, O. M. Gorbenko, D. Litvinov and D. Gerthsen, *Physics of the Solid State*, 2005, **47**, 2213-2218.
12. B. Nikoobakht, X. D. Wang, A. Herzing and J. Shi, *Chemical Society Reviews*, 2013, **42**, 342-365.
13. Y. Chen, D. A. A. Ohlberg and R. S. Williams, *Journal of Applied Physics*, 2002, **91**, 3213-3218.
14. Y. Chen, D. A. A. Ohlberg, G. Medeiros-Ribeiro, Y. A. Chang and R. S. Williams, *Applied Physics Letters*, 2000, **76**, 4004-4006.
15. A. Pradhan, N. Y. Ma and F. Liu, *Physical Review B*, 2004, **70**.
16. A. Li, F. Liu and M. G. Lagally, *Physical Review Letters*, 2000, **85**, 1922-1925.
17. D. J. Eaglesham and M. Cerullo, *Physical Review Letters*, 1990, **64**, 1943.
18. J. Tersoff and R. M. Tromp, *Physical Review Letters*, 1993, **70**, 2782-2785.
19. Z. Zhang, L. M. Wong, H. X. Wang, Z. P. Wei, W. Zhou, S. J. Wang and T. Wu, *Advanced Functional Materials*, 2010, **20**, 2511-2518.
20. Z. Wu, M. G. Hahm, Y. J. Jung and L. Menon, *Journal of Materials Chemistry*, 2009, **19**, 463-467.
21. D. Tsivion, M. Schvartzman, R. Popovitz-Biro, P. von Huth and E. Joselevich, *Science*, 2011, **333**, 1003-1007.
22. R. Bansen, J. Schmidtbauer, R. Gurke, T. Teubner, R. Heimburger and T. Boeck, *Crystengcomm*, 2013, **15**, 3478-3483.
23. U. Bach, D. Lupo, P. Comte, J. E. Moser, F. Weissortel, J. Salbeck, H. Spreitzer and M. Gratzel, *Nature*, 1998, **395**, 583-585.
24. S. U. M. Khan, M. Al-Shahry and W. B. Ingler, *Science*, 2002, **297**, 2243-2245.
25. X. Wang and J. Shi, *Journal of Materials Research*, 2013, **28**, 270-279.
26. G. S. Herman, M. R. Sievers and Y. Gao, *Physical Review Letters*, 2000, **84**, 3354-3357.
27. C. A. Chen, Y. M. Chen, A. Korotcov, Y. S. Huang, D. S. Tsai and K. K. Tiong, *Nanotechnology*, 2008, **19**.
28. S. Chen, M. G. Mason, H. J. Gysling, G. R. Paz-Pujalt, T. N. Blanton, T. Castro, K. M. Chen, C. P. Fictorie, W. L. Gladfelter, A. Franciosi, P. I. Cohen and J. F. Evans, *Journal of Vacuum Science & Technology A*, 1993, **11**, 2419-2429.
29. J.-M. Wu, H. C. Shih and W.-T. Wu, *Journal of Vacuum Science & Technology B*, 2005, **23**, 2122-2126.
30. J.-C. Lee, K.-S. Park, T.-G. Kim, H.-J. Choi and Y.-M. Sung, *Nanotechnology*, 2006, **17**, 4317.
31. X. J. Feng, K. Shankar, O. K. Varghese, M. Paulose, T. J. Latempa and C. A. Grimes, *Nano Letters*, 2008, **8**, 3781-3786.
32. J. C. Lee, K. S. Park, T. G. Kim, H. J. Choi and Y. M. Sung, *Nanotechnology*, 2006, **17**, 4317-4321.
33. K. F. Yu, J. Z. Zhao, Y. P. Guo, X. F. Ding, B. Hari, Y. H. Liu and Z. C. Wang, *Materials Letters*, 2005, **59**, 2515-2518.
34. P. L. Chen, C. T. Kuo, F. M. Pan and T. G. Tsai, *Appl Phys Lett*, 2004, **84**, 3888-3890.
35. C. C. Wang and J. Y. Ying, *Chem Mater*, 1999, **11**, 3113-3120.
36. B. Nikoobakht, S. Eustis and A. Herzing, *The Journal of Physical Chemistry C*, 2009, **113**, 7031-7037.
37. Z. L. Wang, X. Y. Kong and J. M. Zuo, *Phys. Rev. Lett.*, 2003, **91**, 185502.
38. K. Hiruma, M. Yazawa, T. Katsuyama, K. Ogawa, K. Haraguchi, M. Koguchi and H. Kakibayashi, *Journal of Applied Physics*, 1995, **77**, 447-462.
39. D. B. Williams and C. B. Carter, *Transmission Electron Microscopy*, Springer, 2009.
40. B. Nikoobakht, J. Bonevich and A. Herzing, *Journal of Physical Chemistry C*, 2011, **115**, 9961-9969.
41. E. P. A. M. Bakkers, J. A. van Dam, S. De Franceschi, L. P. Kouwenhoven, M. Kaiser, M. Verheijen, H. Wondergem and P. van der Sluis, *Nat Mater*, 2004, **3**, 769-773.
42. S. A. Fortuna and X. L. Li, *Semiconductor Science and Technology*, 2010, **25**, 16.
43. E. P. A. M. Bakkers, M. T. Borgstrom and M. A. Verheijen, *MRS Bulletin*, 2008, **32**, 5.
44. U. Krishnamachari, M. Borgstrom, B. J. Ohlsson, N. Panev, L. Samuelson, W. Seifert, M. W. Larsson and L. R. Wallenberg, *Appl Phys Lett*, 2004, **85**, 2077-2079.